Double-beta decays of light and medium-mass atomic nuclei

Author: Malena Ferrer Aguilera
Facultat de Física, Universitat de Barcelona, Diagonal 645, 08028 Barcelona, Spain.

Advisor: Javier Menéndez, javier.menendez@ub.edu

Abstract: Most atomic nuclei decay via β decay, a weak interaction process. In second-order β decay, two neutrons decay into two protons, accompanied by the emission of two electrons and two antineutrinos. However, if neutrinos were Majorana particles, this would allow the existence of a hypothetical neutrino-less double-β decay ($0\nu\beta\beta$), which violates the symmetries of the Standard Model of particle physics because only two electrons are emitted. In this work, we compute the $0\nu\beta\beta$ decay nuclear matrix elements (NMEs) for light and medium-mass nuclei from ^{6}He to ^{60}Ca. We find larger values of the NMEs for decays where the initial and final nuclei are mirror nuclei. Finally, we find a good correlation between $0\nu\beta\beta$ NMEs and double Gamow-Teller NMEs, which can be measured in nuclear reactions. This correlation is approximately universal for all decays studied.
Keywords: β decay, Standard Model of particle physics, Nuclear Shell Model.
SDGs: Quality education, Industry, innovation, infrastructures.

I. INTRODUCTION

An unstable nucleus decays spontaneously through different mechanisms until it reaches a more stable nucleus, with lower energy. Among these decay mechanisms is β decay, a weak-interaction process.

Single β decay is the conversion inside a nucleus of a nucleon into another nucleon, accompanied by the possible emission of electrons, neutrinos, positrons and antineutrinos. There are three types of β decays: β^-, β^+ and electron capture. This study focuses on β^- decay

$$\beta^- : \qquad n \to p + e^- + \bar{\nu}_e, \tag{1}$$

where n are neutrons, p are protons, e^- are electrons and $\bar{\nu}_e$ are antineutrinos.

Second-order nuclear β^- decay, called two-neutrino double-β decay ($2\nu\beta\beta$) is the conversion inside a nucleus of two neutrons into two protons, accompanied by the emission of two electrons and two antineutrinos

$$2\nu\beta\beta : \qquad 2n \to 2p + 2e^- + 2\bar{\nu}_e, \tag{2}$$

shown in the left diagram of Figure 1. This decay is much less probable than single β^- decay, as it is a second-order process. However, it has been observed in a dozen nuclei with half-lives on the order of 10^{18} years, or longer [2].

The Standard Model of particle physics is the currently accepted theoretical framework that describes the weak interaction. The conserved quantities it imposes for weak interactions are: energy, charge, total angular momentum, baryon number, and lepton number.

In the Standard Model, all massive fermions that carry an electric charge are described by Dirac fields, so they possess distinct particle and antiparticle states. Neutrinos, which are electrically neutral, are the only known fermions for which this distinction is not theoretically required. E. Majorana [1] proposed the alternative that a neutral fermion could be its own antiparticle.

If neutrinos were Majorana particles, this would allow the existence of the hypothetical neutrino-less double-β decay ($0\nu\beta\beta$), which is the conversion of two neutrons into two protons, accompanied by the emission of two electrons with no antineutrinos:

$$0\nu\beta\beta : \qquad 2n \to 2p + 2e^-, \tag{3}$$

shown in the right diagram of Figure 1. Since neutrinos would be their own antiparticles, they would annihilate each other, therefore, only two matter particles ($2e^-$) would be created in the decay. This opens an interesting area of research that could lead to a violation of one of the conserved quantities, lepton number. In addition, Majorana fermions would also help to explain the observed asymmetry between matter and antimatter in the universe.

The half-lives for $0\nu\beta\beta$ follow the equation

$$(T^{0\nu}_{1/2})^{-1} = G_{0\nu}(Q_{\beta\beta}, Z) g_A^4 |M^{0\nu}|^2 m_{\beta\beta}^2, \tag{4}$$

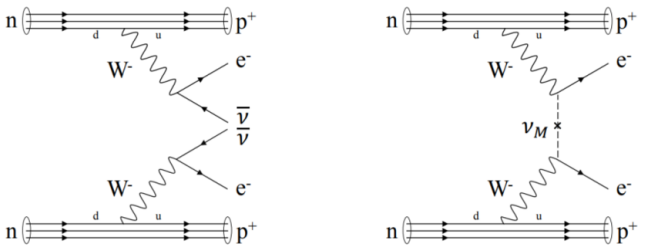

FIG. 1: Diagrams of $2\nu\beta\beta$ (left) and $0\nu\beta\beta$ (right). The diagrams, where the x-axis, from left to right, represents time, show the change of flavor of a d quark to a u quark with straight lines, indicating the decay of a neutron n to a proton p. This change emits two W^- bosons, shown with wavy lines, which decay into two electrons e^- and antineutrinos $\bar{\nu}$. The ν_M cross symbol at the right diagram illustrates the annihilation of two Majorana neutrinos. Figure from [3].

where $G_{0\nu}$ is the emitted electrons' phase-space factor, $Q_{\beta\beta}$ is the Q value for $0\nu\beta\beta$, Z is the number of protons of the initial nucleus, $g_A = 1.27$ is the axial coupling to the nucleon, and $m_{\beta\beta}$ describes the effective neutrino mass, which is a combination of the neutrino masses and mixing parameters [4]. $m_{\beta\beta}$ does not enter $2\nu\beta\beta$ half-lives because for such decays the neutrinos are part of the decay phase-space factor. Finally $M^{0\nu}$ is the $0\nu\beta\beta$ nuclear matrix element (NME).

Since there are no experimental data for $0\nu\beta\beta$, the aim of this work is to theoretically study the $0\nu\beta\beta$ NMEs for ground state to ground state decays of light and medium-mass atomic nuclei with mass number $6 \leq A \leq 60$. For these calculations, we use the nuclear shell model. We also investigate the relation between $0\nu\beta\beta$ NMEs and the NMEs of another process called double Gamow-Teller (DGT) transition, which can be measured in nuclear reactions [4].

II. NUCLEAR SHELL MODEL

Figure 2 shows the energy ordering of the nuclear single-particle orbitals for light and medium-mass nuclei. For particular numbers of neutrons N and protons Z, called magic numbers, the energy gap between single-nucleon orbitals is especially large. Therefore, these orbitals can be thought of as forming energy shells. This is the case for $N = Z = 2, 8$ and 20 in Figure 2.

The shell model was introduced by M. Goeppert-Mayer [5] to explain why the nucleon separation energies present maximum values for nuclei with Z or N equal to magic numbers. This model assumes that the interactions between nucleons are well approximated by a mean field U, which takes the form of a central mean field (harmonic oscillator with $\boldsymbol{l}\cdot\boldsymbol{l}$ term) plus spin-orbit ($\boldsymbol{l}\cdot\boldsymbol{s}$) interactions, where $\boldsymbol{l}$ is the orbital angular momentum and $\boldsymbol{s} = \boldsymbol{\sigma}/2$ the spin:

$$U(r) = \frac{1}{2}m_N\omega^2\boldsymbol{r}^2 + D\boldsymbol{l}\cdot\boldsymbol{l} - C\boldsymbol{l}\cdot\boldsymbol{s}, \tag{5}$$

with m_N the nucleon mass, ω the frequency, $\boldsymbol{r}$ the position and D and C constants [6].

However, in order to better describe atomic nuclei, especially those beyond magic numbers, it is necessary to consider explicitly the nucleon-nucleon interaction, H_{eff}, and to solve the corresponding non-relativistic Schrödinger equation. To derive an easier solution, the nuclear shell model divides the set of orbitals into three groups based on the original shell model of M. Goeppert-Mayer (the lower and upper boundaries of each group of orbitals are magic numbers) [6]:

- Inert core: Fully occupied orbitals.
- Valence space: Available orbitals for the valence nucleons, occupied or not according to H_{eff}.
- External space: The remaining orbitals that are always empty.

In this work we study ground state to ground state decays between states with nuclear angular momentum J and parity P of $J^P = 0^+$ in three valence spaces with three different cores:

- First, the p shell, green box from Figure 2, with orbitals $0p_{1/2}$, $0p_{3/2}$. Its core is the $0s_{1/2}$ orbital.
- The second valence space is the sd shell, blue box from Figure 2, consisting of $0d_{5/2}$, $1s_{1/2}$, and $0d_{3/2}$. Its core contains the p shell and the $0s_{1/2}$ orbital.
- Finally, the pf shell, red box from Figure 2 , with $0f_{7/2}$, $1p_{1/2}$, $1p_{3/2}$ and $0f_{5/2}$ orbitals. Its core consists of the p and sd shells, and the $0s_{1/2}$ orbital.

The single-particle orbitals of each shell are defined as nl_j, where n, l and j are the single-particle principal quantum number, orbital angular momentum and total angular momentum, respectively.

For each valence space with specific H_{eff}, the non-relativistic Schrödinger equation is [6]

$$H_{eff}|\Phi\rangle = E|\Phi\rangle, \tag{6}$$

where the solution wave functions $|\Phi\rangle$ are linear combinations of Slater determinants with amplitude α_i:

$$|\Phi\rangle = \sum_i \alpha_i|\phi_i\rangle, \tag{7}$$

with

$$|\phi_i\rangle = \prod_{i=nljm_j\tau} a_i^\dagger|0\rangle, \tag{8}$$

where i is the single-nucleon state defined by the quantum numbers nl_j, m_j (the angular momentum's projection) and τ (the isospin projection), $a_i^\dagger$ is the creation operator that creates a nucleon in state i of the valence space, and $|0\rangle$ is the vacuum state [7].

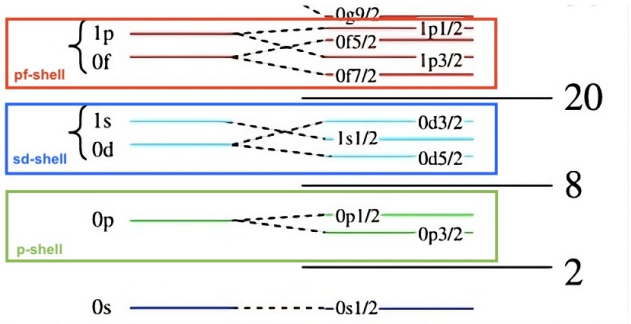

FIG. 2: Nuclear single-particle orbital energy scheme for the shell model, showing the ordering of orbitals including the effect of spin-orbit splitting. The highlighted boxes denote the three spaces studied in this work: the p shell in green, the sd shell in blue and the pf shell in red. Adapted from [8].

The dimension of the configuration space is the product of the combinatorial numbers given by the number of single-particle states for neutrons, N_s, and protons, Z_s, in the valence space, and the valence protons $Z_v = Z - Z_{core}$ and neutrons $N_v = N - N_{core}$. N_{core} and Z_{core} are the number of nucleons in the inert core of each valence space [6]

$$dim = \binom{N_s}{N_v} \cdot \binom{Z_s}{Z_v}. \tag{9}$$

III. INITIAL AND FINAL NUCLEI: LOW-ENERGY SPECTRA

Before computing $0\nu\beta\beta$ NMEs we calculate the eigenstates and corresponding energies for the ground states of all initial and final nuclei. Because all initial and final states we study are nuclei with even N and even Z, their ground state is always $J^P = 0^+$.

Standard diagonalization methods are not usable in large-scale calculations because they demand CPU times that scale exponentially. For example, the ^{12}O configuration space for $J^P = 0^+$ has $dim = 9$ but for ^{56}Ti it has $dim = 14177$, and for this work, we are only interested in a few eigenvalues and eigenvectors. A solution to this problem is using the Lanczos algorithm discussed in [6].

The Lanczos algorithm involves constructing an orthonormal basis through the orthogonalization of the states generated by applying $H_{eff}^N|1\rangle$ to a normalized vector $|1\rangle$, called the "pivot state". Defining E_{11} as $\langle 1|H_{eff}|1\rangle$, and knowing that H_{eff} is Hermitian so $E_{NN-1} = E_{N-1N}$, the Lanczos iterative procedure consists of

$$\begin{aligned} &H_{eff}|N\rangle = E_{NN-1}|N-1\rangle + E_{NN}|N\rangle + E_{NN+1}|N+1\rangle, \\ &E_{NN} = \langle N|H_{eff}|N\rangle. \end{aligned} \tag{10}$$

The equations above show that the Lanczos method builds tridiagonal $N \times N$ matrices, for each step N. This is key because tridiagonal matrices are easy to diagonalize. The algorithm is iterated until the first nuclear states of interest are converged.

We obtain nuclear ground states and their energies using the shell-model code NATHAN [9], which uses the Lanczos algorithm. The H_{eff} that we use are CKI [10] for the p shell, USDB [11] for the sd shell and KB3G [12] for the pf shell. To validate the quality of our calculations, Figure 3 compares our calculated spectra with experimental data [13].

In particular, Figure 3 selects four nuclei in the sd shell: ^{20}O, ^{20}Ne, ^{30}Mg, and ^{30}Si, which correspond to two different $0\nu\beta\beta$ decays with large and small NMEs, see Table II in Appendix B. Figure 3 shows the excitation energies of the first five excited states. Our energy calculations are generally accurate for ^{20}O, ^{20}Ne and ^{30}Si, with an average relative error for the excitation energy of 8%. ^{30}Mg presents the lowest accuracy with an energy

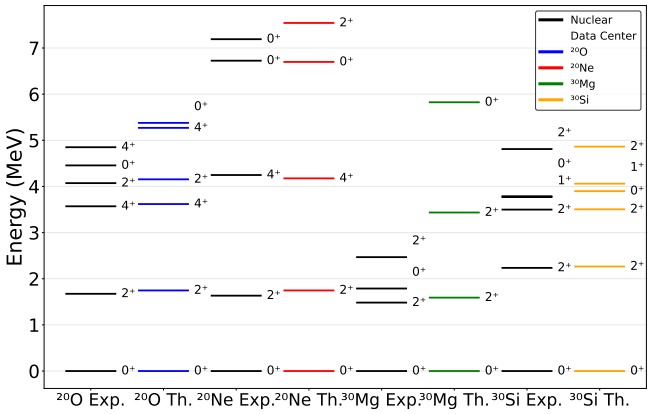

FIG. 3: Calculated energies (Th.) for the ground state and first five excited energy levels with their J^P values for four nuclei in the sd shell, compared to experimental values (Exp.) from [13], shown in black.

relative error of 80%. The accuracy of the excitation energies and ordering of the excited states improves to a 3% and 7%, respectively, if we focus only on the ground and first excited state of those four nuclei. Therefore, we conclude that the calculations are reliable for this work, where we focus on ground states. We expect these results to be representative of all the remaining nuclei we study, since the H_{eff} used are standard interactions used in numerous nuclear structure studies.

IV. NUCLEAR MATRIX ELEMENTS

Once we have obtained the initial $|i\rangle$ and final $\langle f|$ ground states for all $0\nu\beta\beta$ decays studied, we compute the $0\nu\beta\beta$ NMEs introduced at Eq. (4) and the NMEs of DGT transitions between the same nuclei.

A. $0\nu\beta\beta$

For $0\nu\beta\beta$, $M^{0\nu}$ is

$$M^{0\nu} = M^{0\nu}_{GT} - \left(\frac{g_V}{g_A}\right)^2 M^{0\nu}_F + M^{0\nu}_T, \tag{11}$$

where each term corresponds to the matrix element of Gamow-Teller, Fermi and tensor operators in spin space, respectively. $g_V = 1.00$ is the vector coupling to the nucleon [4]. The expressions of the different terms of $M^{0\nu}$ are given by [14]

$$\begin{aligned} M^{0\nu}_{GT} = \frac{2R}{\pi g_A^2} \int_0^\infty |\mathbf{k}| d|\mathbf{k}| \\ \langle f| \sum_{a,b} \frac{j_0\left(|\mathbf{k}| r_{ab}\right) h_{GT}(|\mathbf{k}|) \boldsymbol{\sigma}_a \cdot \boldsymbol{\sigma}_b}{|\mathbf{k}|} \tau_a^+ \tau_b^+ |i\rangle, \end{aligned} \tag{12}$$

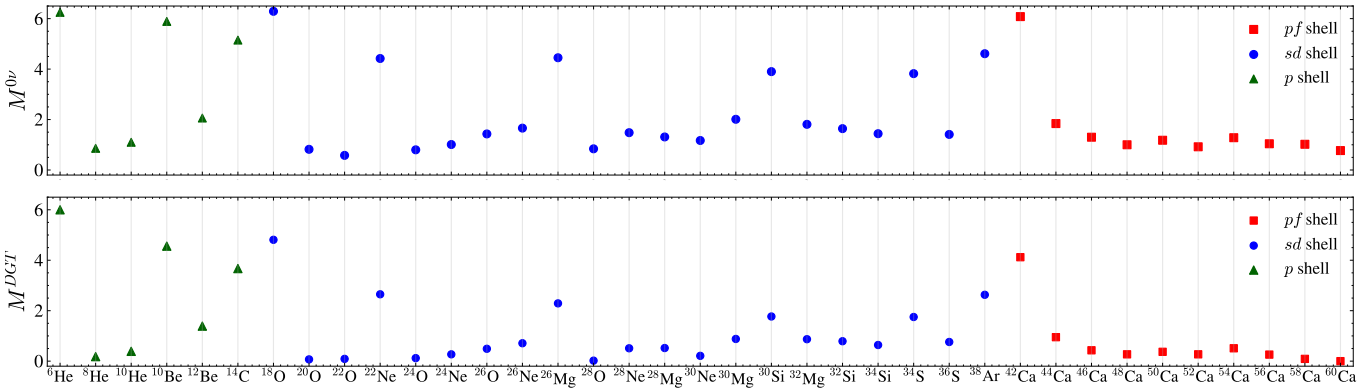

FIG. 4: Top panel: $M^{0\nu}$ values calculated for nuclei in three different shells. The x-axis shows the initial nuclei of each decay. Green triangles represent results for p-shell nuclei, blue circles for sd-shell nuclei and red squares for pf-shell nuclei. Bottom panel: M^{DGT} values obtained for the same nuclei shown with the same symbols. All results are from Tables I, II, and III.

$$M_F^{0\nu} = \frac{2R}{\pi g_A^2}\int_0^\infty |\mathbf{k}|d|\mathbf{k}|\langle f|\sum_{a,b}\frac{j_0\left(|\mathbf{k}|r_{ab}\right)h_F(|\mathbf{k}|)}{|\mathbf{k}|}\tau_a^+\tau_b^+|i\rangle, \tag{13}$$

$$M_T^{0\nu} = \frac{2R}{\pi g_A^2}\int_0^\infty |\mathbf{k}|d|\mathbf{k}|\langle f| \sum_{a,b}\frac{j_2\left(|\mathbf{k}|r_{ab}\right)h_T(|\mathbf{k}|)\left[3\boldsymbol{\sigma}_a\cdot\hat{r}_{ab}\boldsymbol{\sigma}_b\cdot\hat{r}_{ab}-\boldsymbol{\sigma}_a\cdot\boldsymbol{\sigma}_b\right]}{|\mathbf{k}|}\tau_a^+\tau_b^+|i\rangle, \tag{14}$$

where $\boldsymbol{\sigma}_a\cdot\boldsymbol{\sigma}_b$ is the Gamow-Teller operator, $\mathbb{I}$ is the Fermi operator and $[3\boldsymbol{\sigma}_a\cdot\hat{r}_{ab}\boldsymbol{\sigma}_b\cdot\hat{r}_{ab}-\boldsymbol{\sigma}_a\cdot\boldsymbol{\sigma}_b]$ is the tensor operator. Subindices a, b sum over all neutrons in the nucleus, $\mathbf{k}$ is the momentum transfer in the $0\nu\beta\beta$, τ^+ is the isospin raising operator that turns neutrons into protons, j_i are spherical Bessel functions, and r_{ab} is the distance between neutrons a and b. h_{GT}, h_F, and h_T are the neutrino potentials defined in Appendix A, and R is the nuclear radius [4]

$$R = 1.2A^{1/3}\text{fm}. \tag{15}$$

In order to obtain $M^{0\nu}$ for every decay, we compute $M_{GT}^{0\nu}$, $M_F^{0\nu}$ and $M_T^{0\nu}$ using the NATHAN code [9].

B. Double Gamow-Teller transitions

An accurate calculation of the $0\nu\beta\beta$ NMEs is challenging, as the nuclear shell model handles large configuration spaces. The uncertainty associated with these calculations makes it difficult to extract $m_{\beta\beta}$ values from half-life measurements. In this context, DGT transitions emerge as a possible analog to $0\nu\beta\beta$. They are second-order and share the same spin and isospin structure as $M_{GT}^{0\nu}$ in Eq. (12). As an advantage, their NME:

$$M^{DGT} = \langle f|\boldsymbol{\sigma}_a\cdot\boldsymbol{\sigma}_b\tau_a^+\tau_b^+|i\rangle, \tag{16}$$

is easier to compute, as it only involves the simpler two-body Gamow-Teller operator, $\boldsymbol{\sigma}_a\cdot\boldsymbol{\sigma}_b$, and can be measured in nuclear reactions.

Thus, computing DGT NMEs can serve as a proxy to estimate $M^{0\nu}$. If a model reproduces M^{DGT} well, it can be more reliable for predicting $M^{0\nu}$. Therefore, we compute M^{DGT} for the same ground state to ground state transitions in the three shell-model valence spaces considered for $0\nu\beta\beta$, and compare the results obtained.

V. RESULTS AND DISCUSSION

The upper panel of Figure 4 shows the $M^{0\nu}$ values for all nuclei studied in this work, including the decays of p-shell (green triangles), sd-shell (blue circles) and pf-shell (red squares) nuclei. Likewise, the lower panel of Figure 4 shows the M^{DGT} values for the same nuclei with the same symbols. A first interesting result is that some values of both $M^{0\nu}$ and M^{DGT} are significantly larger than others. These larger NMEs correspond to decays where the initial and final nuclei are mirror nuclei, which means that the initial and final nuclei have the number of protons and neutrons exchanged. The energy spectra of mirror nuclei are almost identical and they also share the same total isospin T [7]:

$$T = \frac{|N-Z|}{2}. \tag{17}$$

In the results shown in the top panel of Figure 4, we observe no clear relationship between $M^{0\nu}$ and A for each decay. This indicates that the observed behavior is predominantly governed by T and spin degrees of freedom. For nuclei in all three valence spaces, decays where initial and final states do not have the same T value have NME values in the range $0 \leq M^{0\nu} \leq 2$ with no clear pattern. Comparing the results in the bottom panel of Figure 4, the general behavior for M^{DGT} is similar. Interestingly, transitions with large (small) $M^{0\nu}$ values are also associated with large (small) M^{DGT} values as well.

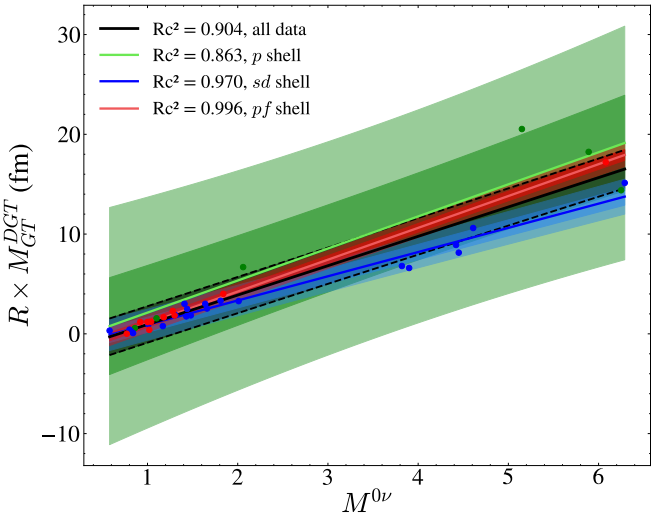

FIG. 5: $R \times M^{DGT}$ as a function of $M^{0\nu}$ for decays in three different valence spaces (p shell in green, sd shell in blue and pf shell in red). In addition to the results for each decay studied (circles), the figure shows the best linear fit as solid lines and correlation coefficients R_c, and the corresponding 68% (dark-colored bands) and 95% (light-colored bands) CL prediction bands. The best linear fit to the combined results for all calculated nuclei is shown with a solid black line and its 68% CL prediction band with a dashed black line.

Finally, we analyze the correlation between $0\nu\beta\beta$ and DGT NMEs. Figure 5 represents the values of M^{DGT} for all transitions studied in this work, multiplied by R, as a function of $M^{0\nu}$ for the same nuclei. The reason for multiplying by R is that this factor is included in the definition of $M^{0\nu}$, see Eqs. (12)-(14).

Figure 5 shows the theoretical results from the three Tables I , II, and III in Appendix B, with the p-shell theoretical results in green, sd-shell ones in blue and pf-shell ones in red. Figure 5 shows, in addition to the results of each individual calculation, the best linear fit and 68% (dark-colored bands) and 95% (light-colored bands) confidence level (CL) prediction bands.

Qualitatively, Figure 5 indicates that the correlation between $0\nu\beta\beta$ and DGT NMEs is very good, and all correlation coefficients Rc^2 obtained quantify this conclusion. The best fit obtained is for the pf shell with $Rc^2 = 0.996$. The lowest Rc^2 obtained is for the p shell with $Rc^2 = 0.863$. This lower value may be related to having only six decays in this valence space, half of which are between mirror nuclei. All three fits are very similar for small NME values and start to differ once $M^{0\nu}$ grows.

Finally, Figure 5 shows in black the best fit and its 68% CL prediction band when considering all decays studied in this work, with $Rc^2 = 0.904$. The 68% black band overlaps with the other 68% CL bands, except slightly with the sd one for large NME values. Therefore, this overall correlation is consistent with the ones for the individual valence spaces.

VI. CONCLUSIONS

In this work, we computed the NME values of $M^{0\nu}$ and M^{DGT} using the nuclear shell model. The reliability of the wavefunctions was validated by comparing them to data of energy spectra, with relative errors in the range of 3-7%. Moreover, the obtained $M^{0\nu}$ results are important for obtaining theoretical $m_{\beta\beta}$ values which will help us understand neutrinos.

An initial look at the results showed no clear pattern for either NME with mass number, but we found the largest NMEs occurred where the initial and final nuclei were mirror nuclei. We found a strong correlation ($Rc^2 = 0.904$) between the DGT and $0\nu\beta\beta$ NMEs, this result suggests a universal correlation between the NMEs of these two processes. This processes, and helps to test $0\nu\beta\beta$ calculations through experimentally accessible DGT reactions.

Acknowledgments

I would like to express my gratitude to my advisor, Javier Menéndez, for all his guidance and advice throughout this work and Daniel Castillo, who also assisted through it. Special thanks to my family and friends who supported me through the journey.

[1] E. Majorana. *Il Nuovo Cim.*, **14**, 171. (1937)
[2] A. S. Barabash. *Universe*, **6**, 159. (2020)
[3] C. Goufu. *PoS*, **HQL2018**, 054. (2018)
[4] M. Agostini, G. Benato, J. A. Detwiler, A. Jason, J. Menéndez, *Rev. Mod. Phys.*, **95**, 025002. (2023)
[5] M. Goeppert, H. Jensen, "Elementary Theory of Nuclear Shell Structure". John Wiley & Sons. (1995)
[6] A. Poves, F. Nowacki. "The nuclear shell model." Springer. (2001)
[7] J. Suhonen. "From Nucleons to Nucleus. Concepts of Microscopic Nuclear Theory." Springer. (2007)
[8] N. Wallet. Physics Libretexts. (2024) phys.libretexts.org
[9] E. Caurier, G. Martínez-Pinedo, F. Nowacki, A. Poves, A. P. Zuker. *Rev. Mod. Phys.*, **77**, 427. (2005)
[10] S. Cohen, D. Kurath. *Nuc. Phys.*, **89**, 707. (1965)
[11] B. A. Brown, W. Richter, *Phys. Rev. C.*, **74**, 11. (2006)
[12] A. Poves, J. Sánchez Solano, E. Caurier, F. Nowacki. *Nucl. Phys. A*, **694**, 157. (2001)
[13] National Nuclear Data Center, Brookhaven National Laboratory. (2025) www.nndc.bnl.gov
[14] P. Soriano. "Impact of ultrasoft neutrinos and realistic radial wavefunctions on neutrinoless double-beta decay matrix elements." *UB*. (2020)

Desintegracions doble beta de nuclis atòmics lleugers i de massa mitjana

Author: Malena Ferrer Aguilera
Facultat de Física, Universitat de Barcelona, Diagonal 645, 08028 Barcelona, Spain.

Advisor: Javier Menéndez, javier.menendez@ub.edu

La majoria dels nuclis atòmics es desintegren mitjançant la desintegració β, un procés d'interacció feble. En la desintegració β de segon ordre, dos neutrons es transformen en dos protons, acompanyats de l'emissió de dos electrons i dos antineutrins. Tanmateix, si els neutrins fossin partícules de Majorana, això permetria l'existència d'una hipotètica desintegració doble-β sense neutrins ($0\nu\beta\beta$), que viola les simetries del Model Estàndard de la física de partícules, ja que només s'emeten dos electrons. En aquest treball, calculem els elements de matriu nuclears (NME) de la desintegració $0\nu\beta\beta$ per a nuclis lleugers i de massa mitjana, des de ^{6}He fins a ^{60}Ca. Trobem valors més grans dels NME per a desintegracions en què els nuclis inicial i final són nuclis mirall. Finalment, trobem una bona correlació entre els NME de la $0\nu\beta\beta$ i els NME de les transicions doble Gamow-Teller, que es poden mesurar en reaccions nuclears. Aquesta correlació és aproximadament universal per a totes les desintegracions estudiades.

Paraules clau: Desintegracions β, Model estàndard de física de partícules, Model de capes nuclear.
ODSs: Educació de qualitat. Indústria, innovació, infraestructures.

Objectius de Desenvolupament Sostenible (ODSs o SDGs)

1. Fi de les desigualtats		10. Reducció de les desigualtats	
2. Fam zero		11. Ciutats i comunitats sostenibles	
3. Salut i benestar		12. Consum i producció responsables	
4. Educació de qualitat	X	13. Acció climàtica	
5. Igualtat de gènere		14. Vida submarina	
6. Aigua neta i sanejament		15. Vida terrestre	
7. Energia neta i sostenible		16. Pau, justícia i institucions sòlides	
8. Treball digne i creixement econòmic		17. Aliança pels objectius	
9. Indústria, innovació, infraestructures	X		

Appendix A: Neutrino potentials

The functions h_i are the neutrino potentials defined as

$$h_{GT}(|\mathbf{k}|) \equiv g_A^2\left(\mathbf{k}^2\right) - \frac{g_A^2\left(\mathbf{k}^2\right) g_P^2\left(\mathbf{k}^2\right)\mathbf{k}^2}{3m_N} + \frac{g_P^2\left(\mathbf{k}^2\right)\mathbf{k}^4}{12m_N^2} + \frac{g_M^2\left(\mathbf{k}^2\right)\mathbf{k}^2}{6m_N^2}, \tag{A1}$$

$$h_F(|\mathbf{k}|) \equiv \frac{g_V^2\left(\mathbf{k}^2\right)}{g_A^2}, \tag{A2}$$

$$h_T(|\mathbf{k}|) \equiv \frac{g_A^2\left(\mathbf{k}^2\right) g_P^2\left(\mathbf{k}^2\right)\mathbf{k}^2}{3m_N} - \frac{g_P^2\left(\mathbf{k}^2\right)\mathbf{k}^4}{12m_N^2} + \frac{g_M^2\left(\mathbf{k}^2\right)\mathbf{k}^2}{12m_N^2}, \tag{A3}$$

obtained from [14], where g_M and g_P are the magnetic and induced pseudoscalar couplings. The couplings have a momentum dependence described as dipole form factors

$$\begin{aligned} g_V\left(\boldsymbol{q}^2\right) &= \left[1+\boldsymbol{q}^2/\Lambda_V^2\right]^{-2}, \\ g_A\left(\boldsymbol{q}^2\right) &= \left[1+\boldsymbol{q}^2/\Lambda_A^2\right]^{-2}, \\ g_M\left(\boldsymbol{q}^2\right) &= \left(1+\mu_p-\mu_n\right) g_V\left(\boldsymbol{q}^2\right), \\ g_P\left(\boldsymbol{q}^2\right) &= 2m_N g_A\left(\boldsymbol{q}^2\right)\frac{1}{\boldsymbol{q}^2+m_\pi^2}, \end{aligned} \tag{A4}$$

where $\Lambda_V = 850$ MeV and $\Lambda_A = 1040$ MeV are the vector and axial masses, μ_p - $\mu_n = 3.70$ is the isovector anomalous magnetic moment of the nucleon and $m_\pi = 138.07$ MeV is the pion mass.

Appendix B: $0\nu\beta\beta$ and DGT NME

Decay	$M^{0\nu}$	$M^{0\nu}_{GT}$	$M^{0\nu}_{F}$	$M^{0\nu}_{T}$	M^{DGT}
^{6}He $\rightarrow$ ^{6}Be	6.25	5.10	1.15	0.00	6.00
^{8}He $\rightarrow$ ^{8}Be ^{8}Be $\rightarrow$ ^{8}C	0.86	0.73	0.13	0.01	0.18
^{10}He $\rightarrow$ ^{10}Be ^{10}C $\rightarrow$ ^{10}O	1.10	0.95	0.14	0.01	0.39
^{10}Be $\rightarrow$ ^{10}C	5.89	4.64	1.29	0.04	4.56
^{12}Be $\rightarrow$ ^{12}C ^{12}C $\rightarrow$ ^{12}O	2.06	1.86	0.17	0.03	1.39
^{14}C $\rightarrow$ ^{14}O	5.15	3.97	1.32	0.14	3.67

TABLE I: $0\nu\beta\beta$ NMEs (second column) and DGT matrix elements (sixth column) for the transitions of several p-shell nuclei. The Gamow-Teller, Fermi and tensor components of $M^{0\nu}$ are given in the third, fourth and fifth columns, respectively.

$0\nu\beta\beta$ Decay	$M^{0\nu}$	$M^{0\nu}_{GT}$	$M^{0\nu}_{F}$	$M^{0\nu}_{T}$	M^{DGT}
^{18}O $\rightarrow$ ^{18}Ne	6.29	5.03	1.33	0.07	4.80
^{20}O $\rightarrow$ ^{20}Ne ^{20}Ne $\rightarrow$ ^{20}Mg	0.82	0.71	0.15	0.03	0.07
^{22}O $\rightarrow$ ^{22}Ne ^{22}Mg $\rightarrow$ ^{22}Si	0.58	0.49	0.12	0.03	0.09
^{22}Ne $\rightarrow$ ^{22}Mg	4.42	3.19	1.30	0.08	2.65
^{24}O $\rightarrow$ ^{24}Ne ^{24}Si $\rightarrow$ ^{24}S	0.80	0.67	0.12	0.00	0.12
^{24}Ne $\rightarrow$ ^{24}Mg ^{24}Mg $\rightarrow$ ^{24}Si	1.01	0.88	0.12	0.04	0.27
^{26}O $\rightarrow$ ^{26}Ne ^{26}S $\rightarrow$ ^{26}Ar	1.43	1.21	0.16	0.06	0.49
^{26}Ne $\rightarrow$ ^{26}Mg ^{26}Si $\rightarrow$ ^{26}S	1.66	1.46	0.20	0.01	0.71
^{26}Mg $\rightarrow$ ^{26}Si	4.45	3.14	1.40	0.09	2.30
^{28}O $\rightarrow$ ^{28}Ne ^{28}Ar $\rightarrow$ ^{28}Ca	0.84	0.66	0.12	0.07	0.02
^{28}Ne $\rightarrow$ ^{28}Mg ^{28}S $\rightarrow$ ^{28}Ar	1.48	1.27	0.17	0.05	0.51
^{28}Mg $\rightarrow$ ^{28}Si ^{28}Si $\rightarrow$ ^{28}S	1.31	1.15	0.16	0.00	0.52
^{30}Ne $\rightarrow$ ^{30}Mg ^{30}Ar $\rightarrow$ ^{30}Ca	1.17	0.96	0.14	0.07	0.21
^{30}Mg $\rightarrow$ ^{30}Si ^{30}S $\rightarrow$ ^{30}Ar	2.01	1.73	0.21	0.06	0.88
^{30}Si $\rightarrow$ ^{30}S	3.90	2.66	1.39	0.15	1.77
^{32}Mg $\rightarrow$ ^{32}Si ^{32}Ar $\rightarrow$ ^{32}Ca	1.81	1.61	0.16	0.05	0.87
^{32}Si $\rightarrow$ ^{32}S ^{32}S $\rightarrow$ ^{32}Ar	1.64	1.50	0.20	0.06	0.79
^{34}Si $\rightarrow$ ^{34}S ^{34}Ar $\rightarrow$ ^{34}Ca	1.44	1.27	0.17	0.00	0.64
^{34}S $\rightarrow$ ^{34}Ar	3.82	2.58	1.42	0.18	1.75
^{36}S $\rightarrow$ ^{36}Ar ^{36}Ar $\rightarrow$ ^{36}Ca	1.41	1.30	0.19	0.09	0.76
^{38}Ar $\rightarrow$ ^{38}Ca	4.61	3.35	1.47	0.21	2.63

TABLE II: Same as Table I but for *sd*-shell nuclei.

$0\nu\beta\beta$	$M^{0\nu}$	$M^{0\nu}_{GT}$	$M^{0\nu}_{F}$	$M^{0\nu}_{T}$	M^{DGT}
^{42}Ca $\rightarrow$ ^{42}Ti	6.08	4.76	1.43	0.11	4.12
^{44}Ca $\rightarrow$ ^{44}Ti	1.84	1.69	0.22	0.07	0.95
^{46}Ca $\rightarrow$ ^{46}Ti	1.30	1.18	0.19	0.07	0.43
^{48}Ca $\rightarrow$ ^{48}Ti	1.00	0.91	0.15	0.06	0.27
^{50}Ca $\rightarrow$ ^{50}Ti	1.18	1.02	0.15	0.00	0.37
^{52}Ca $\rightarrow$ ^{52}Ti	0.92	0.80	0.12	0.00	0.27
^{54}Ca $\rightarrow$ ^{54}Ti	1.28	1.13	0.13	0.03	0.51
^{56}Ca $\rightarrow$ ^{56}Ti	1.04	0.89	0.12	0.03	0.26
^{58}Ca $\rightarrow$ ^{58}Ti	1.02	0.82	0.13	0.07	0.09
^{60}Ca $\rightarrow$ ^{60}Ti	0.77	0.60	0.11	0.06	0.00

TABLE III: Same as Table I but for pf-shell nuclei.